Original Article

Oxidative stress induces EGFR inhibition-related skin cell death

Midori Morita,[1] Mahiro Iizuka-Ohashi,[1,*] Motoki Watanabe,[2] Takumi Narita,[2] Chikage Kato,[1] Daichi Kakibuchi,[1] Fuyuki Kitano,[1] Yoshimi Ouchi,[3] Koichi Sakaguchi,[1] and Tetsuya Taguchi[1]

[1]Division of Endocrine and Breast Surgery and [2]Department of Molecular-Targeting Prevention, Kyoto Prefectural University of Medicine, 465 Kajii-cho, Kamigyo-ku, Kyoto, Japan
[3]Department of Surgery, Saiseikai Shiga Hospital, 2-4-1 Ohashi, Ritto, Shiga, Japan

(Received 7 July, 2020; Accepted 24 November, 2020; Published online 25 March, 2021)

Cutaneous side effects are often observed in patients treated with chemotherapeutic agents, including those treated with epidermal growth factor receptor (EGFR) inhibitors. These side effects are not fatal but often require dose reduction of chemotherapies. The mechanisms of epidermal growth factor receptor inhibition-related dermatologic toxicities are unclear, and prophylactic approaches are not well-established. To explore the mechanisms of the cutaneous side effects induced by epidermal growth factor receptor inhibition, we analyzed the metabolome using human keratinocyte cells. We first demonstrated that afatinib and lapatinib induced apoptosis in HaCaT cells. Using liquid chromatography-mass spectrometry, we detected 676 and 482 metabolites and compounds in the cells and media, respectively. We observed diverse metabolic alterations, including glycolysis, TCA metabolism, and polyamine metabolism, and also found a change in glutathione metabolites after epidermal growth factor receptor inhibition, which led to the accumulation of reactive oxygen species. Supplementation of *N*-acetyl cysteine partly rescued the afatinib-induced apoptosis, suggesting that reactive oxygen species are involved in the cytotoxicity of skin cells. We observed epidermal growth factor receptor inhibitor-associated comprehensive metabolic changes in human keratinocyte cells, suggesting that oxidative stress evokes cutaneous side effects induced by EGFR inhibition.

***Key Words*: EGFR inhibitor, cutaneous side effect, metabolomics, reactive oxygen species, apoptosis**

The epidermal growth factor receptor (EGFR) is a tyrosine kinase receptor belonging to the ErbB family, known to be involved in several signaling pathways such as the RAF/MEK, JAK/STAT, and PI3K/Akt pathways.[1,2] Those pathways are responsible for cell proliferation, survival, and migration.[1,3] Mutations or overexpression of EGFR have been observed in 40–80% of lung cancer, 14–91% of breast cancer, 33–74% of stomach cancer, 25–77% of colon cancer, 35–50% of pancreatic cancer, 40–80% of prostate cancer, 50–90% of kidney cancer, 35–70% of ovarian cancer, and 36–100% of head and neck cancer cases.[4–6] Moreover, overexpression of EGFR is considered to be related to poor prognosis.[7] Thus, EGFR is a favorable target for suppressing cancer growth, with EGFR-targeting agents including tyrosine kinase receptor inhibitors and monoclonal antibodies. Although anti-EGFR agents have shown beneficial effects in many patients with cancer,[4,5] these patients often experience adverse effects, which may preclude the treatment process.

Among the most common adverse effects of administration of EGFR inhibitors are cutaneous toxicities.[8] The major cutaneous toxicities are inflammatory papulopustular rash (60–90%), bacterial infections (38–70%), and dry and itchy skin (12–16%).[8–10] These symptoms are not fatal or irreversible but they affect and impair the quality of life of patients. Importantly, dermatologic toxicities, the grade of which has been positively correlated with the efficacies of EGFR inhibitors,[8,11,12] are dose-limiting factors of EGFR inhibitors. Therefore, management of the EGFR inhibitor-related cutaneous adverse effects is indispensable for ensuring treatment quality. However, palliative approaches, including steroid or moisturizing ointments, are the only choices for alleviating skin inflammation.

The mechanisms of the EGFR inhibition-related dermatologic toxicities are not fully understood. Among the components of the skin cell architecture, keratinocyte cells in the basal cell layer express higher levels of EGFR compared to cells in the suprabasal cell layer. For instance, in mice in which epidermal EGFR expression was knocked down in keratinocyte cells, skin damages similar to that in patients treated with EGFR inhibitors was observed.[13,14] Hence, keratinocyte cells were considered as responsible for these skin symptoms.[8] Once keratinocyte proliferation is disturbed, the cell structure of the normal skin collapses. Eventually, the important skin cell barrier function is lost, accompanied by loss of body fluids and susceptibility to infection. Damaged keratinocyte cells also release chemokines and cytokines, some of which induce local inflammation in the skin.[15,16] To better understand cytotoxicity in EGFR inhibitor-treated skin cells, we performed metabolome analysis. Inhibition of EGFR was found to induce various metabolic perturbations in human keratinocytes HaCaT cells. We focused on alterations in glutathione metabolites, which suggested promotion of the induction of reactive oxygen species (ROS) and suppression of ROS scavenging after treatment with an EGFR inhibitor. We confirmed that EGFR inhibition led to the accumulation of ROS in keratinocyte cells, which was partly responsible for apoptosis in skin cells. Our findings revealed that oxidative stress was at least partially involved in apoptosis induced by EGFR inhibitors in skin cells, which may lead to new approaches for managing and preventing this cutaneous side effect by using ROS scavengers.

Materials and Methods

Cell culture and reagents. Human skin immortalized keratinocyte HaCaT cells (Cell Lines Service GmbH, Eppelneim, Germany) were cultured in Dulbecco's Modified Eagle Medium containing L-glutamine (Nacalai Tesque, Kyoto, Japan) supplemented with 10% fetal bovine serum (Biowest, Nuaille,

*To whom correspondence should be addressed.
E-mail: iom0220@koto.kpu-m.ac.jp

doi: 10.3164/jcbn.20-112

France) and antibiotics (100 U/ml penicillin-streptomycin and 5 ng/ml amphotericin B) (Nacalai Tesque). The cells were incubated at 37°C in a humidified atmosphere of 5% CO_2. Afatinib was purchased from Selleck Chemicals (Houston, TX), and lapatinib was obtained from Sigma-Aldrich (St. Louis, MO). These agents were dissolved in dimethyl sulfoxide (Nacalai Tesque).

Cell growth assay. Cells were seeded into 96-well plates at a density of 2,000 cells per well. Varying concentrations of afatinib and lapatinib were added to cells at 24 h after plating and the cells were further incubated for 72 h, followed by the Cell Counting Kit-8 assay (CCK8; Dojindo, Kumamoto, Japan). After an additional 4 h of incubation with the CCK-8 reagent, the absorbance of samples at 450 nm was measured with a microplate reader (Multiskan FC; Thermo Fisher Scientific, Waltham, MA).

Analysis of apoptosis. Apoptosis was evaluated by flow cytometry using a FACSCalibur system (BD Biosciences, Franklin Lakes, NJ) as previously described.[17] Briefly, cells were seeded at a density of 1×10^5 cells per well into 6-well plates and incubated for 24 h, and then treated with the indicated agents for 72 h. We used 0.1% Triton X-100 (Nacalai Tesque) and 25 μg/ml propidium iodide (Sigma-Aldrich) to stain the cells. A total of 1×10^4 cells was counted in each experiment. DNA fragmentation was quantified by measuring the percentage of cells with hypodiploid DNA as the sub-G1 population. These data were analyzed using Cell Quest and Modifit LT software (BD Biosciences).

Western blotting. Cells were harvested and lysed in Laemmli buffer (62.5 mM Tris-HCl, 2% sodium dodecyl sulfate, 25% glycerol, 0.01% bromophenol blue). The cell lysates were sonicated and centrifuged at 20,400 *g* for 20 min at 4°C, and the supernatant was collected. Equal amounts of the protein extract were subjected to sodium dodecyl sulfate-polyacrylamide gel electrophoresis on 10% precast polyacrylamide gels (Bio-Rad, Hercules, CA) and transferred to a polyvinylidene fluoride membrane (Millipore, Billerica, MA). The following primary antibodies were used: rabbit polyclonal anti-poly (ADP-ribose) polymerase (PARP; 1:1,000, Cell Signaling Technology, Danvers, MA) and mouse mono-clonal anti-β-actin (1:1,000, Sigma-Aldrich). Signals were detected with a Chemi-Lumi One L (Nacalai Tesque).

Metabolome analysis. Metabolome analysis was performed by Metabolon, Inc. (Durham, NC). Cells were grown under the indicated culture conditions and treated with afatinib and lapatinib (10 μM) for 6 and 18 h. Next, 100 μl packed cell pellets and 200 μl culture supernatants were harvested separately, flash-frozen in liquid nitrogen, and stored at −80°C. Each sample was accessioned into the Metabolon Laboratory Information Management System (LIMS) and assigned a unique identifier, which was only associated with the original source identifier. This identifier was used to track all sample handling, tasks, results, and other steps. Samples were tracked by the LIMS system. All portions of any sample were automatically assigned unique identifiers by the LIMS when a new task was created; the relationship of these samples was also tracked. All samples were maintained at −80°C until processing.

Samples were prepared using the automated MicroLab STAR system from Hamilton Company (Salt Lake City, UT). Recovery standards were added prior to the first step in the extraction process for quality control purposes. To remove proteins, small molecules bound to protein or trapped in the precipitated protein matrix were dissociated; to recover chemically diverse metabolites, proteins were precipitated with methanol under vigorous shaking for 2 min followed by centrifugation. The resulting extract was divided into 5 fractions: 2 for analysis using 2 separate reverse phase/ultra-performance liquid chromatography (UPLC)-tandem mass spectrometry (MS/MS) methods with positive ion mode electrospray ionization, 1 for analysis using reverse phase/UPLC-MS/MS with negative ion mode electrospray ionization, 1 for analysis using hydrophilic interaction/UPLC-MS/MS with negative ion mode electrospray ionization, and 1 sample was reserved as a backup. Samples were placed briefly on a TurboVap® (Zymark, Palo Alto, CA) to remove the organic solvent. Sample extracts were stored overnight under nitrogen before preparation for analysis.

Data extraction from the raw mass spectrometry data files yielded information that could be loaded into a relational database. Once in the database, the information was examined and appropriate quality control limits were imposed. Peaks were identified using proprietary peak integration software from Metabolon. Compounds were identified by comparison to library entries of purified standards or recurrent unknown entities. Identification of known chemical entities was based on comparison with metabolomic library entries of purified standards.

Pathway enrichment analysis. Pathway enrichment analysis was performed using the metabolon system to visualize the number of statistically significantly different compounds relative to all detected compounds in a sub-pathway, compared to the total number of significantly different compounds relative to all detected compounds in the study. A pathway enrichment value greater than one indicates that the pathway contains more significantly changed compounds relative to the study overall, suggesting that the pathway is a target of interest and should be further investigated. The pathway enrichment value was calculated as follows:

$$\text{Enrichment value} = (k/m)/((n - k)/(N - m))$$

where m is the number of metabolites in the pathway, k is the number of significant metabolites in the pathway, n is the total number of significant metabolites, and N is the total number of metabolites.

Oxidized glutathione (GSSG)/reduced glutathione (GSH) quantification analysis. We quantified intracellular GSH and GSSG using a GSSG/GSH quantification kit (Dojindo). After co-incubation with afatinib or lapatinib (0.1, 1 μM) for 18 h, the cells were collected and processed according to the manufacturer's protocol. Briefly, the cells were washed and centrifuged at 200 *g* for 5 min at 4°C. The cell pellets were mixed with 80 μl HCl (10 mM) and homogenized by freezing and thawing twice. After centrifugation at 8,000 *g* for 10 min at 4°C, the samples were diluted with 5-sulfosalicylic acid and incubated with the kit buffer solution at 37°C. After a further 10-min incubation with the kit working solution, the absorbance of the samples at 415 nm was measured using a microplate reader.

Analysis of accumulation of ROS. As reported previously,[18] the cells were seeded at a density of 4×10^5 cells per well in 6-well plates and cultured for 2 days. Cells were subsequently incubated for 6 h in Dulbecco's Modified Eagle Medium containing 10 μM afatinib or lapatinib. After incubation, the cells were immersed in fresh culture medium with 10 μM CM-H2DCFDA (Thermo Fisher Scientific) at 37°C for 30 min. The cells were harvested by trypsinization, centrifuged at 500 × *g* for 5 m, washed twice with PBS (Nacalai Tesque), and mixed with fresh PBS. Flow cytometry analysis was carried out with a FACSCalibur. A total of 1×10^4 cells was counted in each experiment. These data were analyzed with Cell Quest and Modifit LT software.

Statistical analysis. The results are presented as the mean ± SD. In metabolome analysis, analysis of variance and Welch's two-sample *t* test were used to identify biochemicals that differed significantly between experimental groups, with *p* values less than 0.10 considered as statistically significant. Unless otherwise specified, the statistical difference of means between 2 groups was assessed by unpaired Student's *t* test, and *p* values less than 0.05 were considered as statistically significant.

doi: 10.3164/jcbn.20-112

Results

EGFR inhibitors inhibited cell growth in human keratinocyte HaCaT cells. To investigate the cytotoxicity of EGFR inhibitors towards skin cells, we treated keratinocyte HaCaT cells with two types of EGFR inhibitors, the irreversible inhibitor afatinib (Fig. 1A) and reversible inhibitor lapatinib (Fig. 1B), for 72 h. Cell growth assays showed that EGFR inhibition dose-dependently inhibited cell growth. The half maximal inhibitory concentrations of afatinib and lapatinib were 0.2 nM and 0.2 μM, respectively.

EGFR inhibitors induced apoptosis in HaCaT cells. To clarify the mechanisms of EGFR inhibitor-induced suppression of cell growth, we performed flow cytometric analysis.

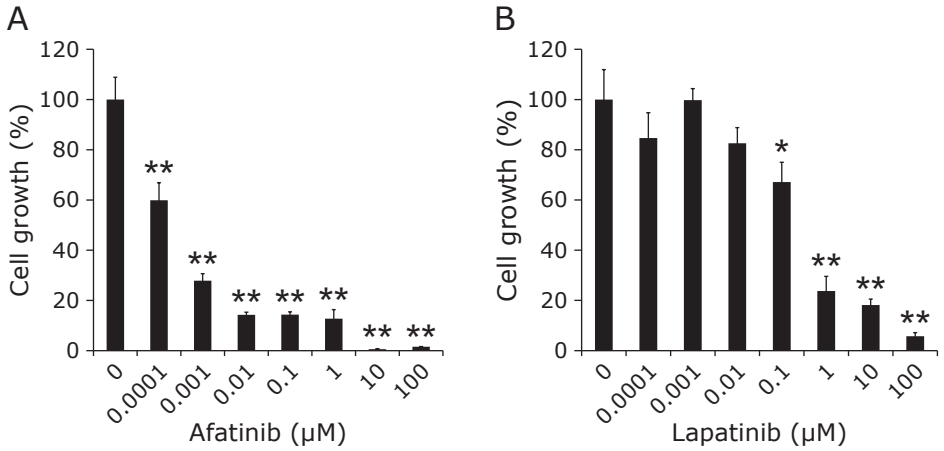

Fig. 1. EGFR inhibitors suppress cell growth of human keratinocytes. Growth inhibitory effect of afatinib or lapatinib on HaCaT cells. Cells were treated with afatinib (A) or lapatinib (B) at the indicated concentrations for 72 h, and cell viability was measured in a Cell Counting Kit-8 assay. Each data point obtained with dimethyl sulfoxide considered as 100%. Columns, means of triplicate data; bars, SD; *p<0.05, **p<0.01.

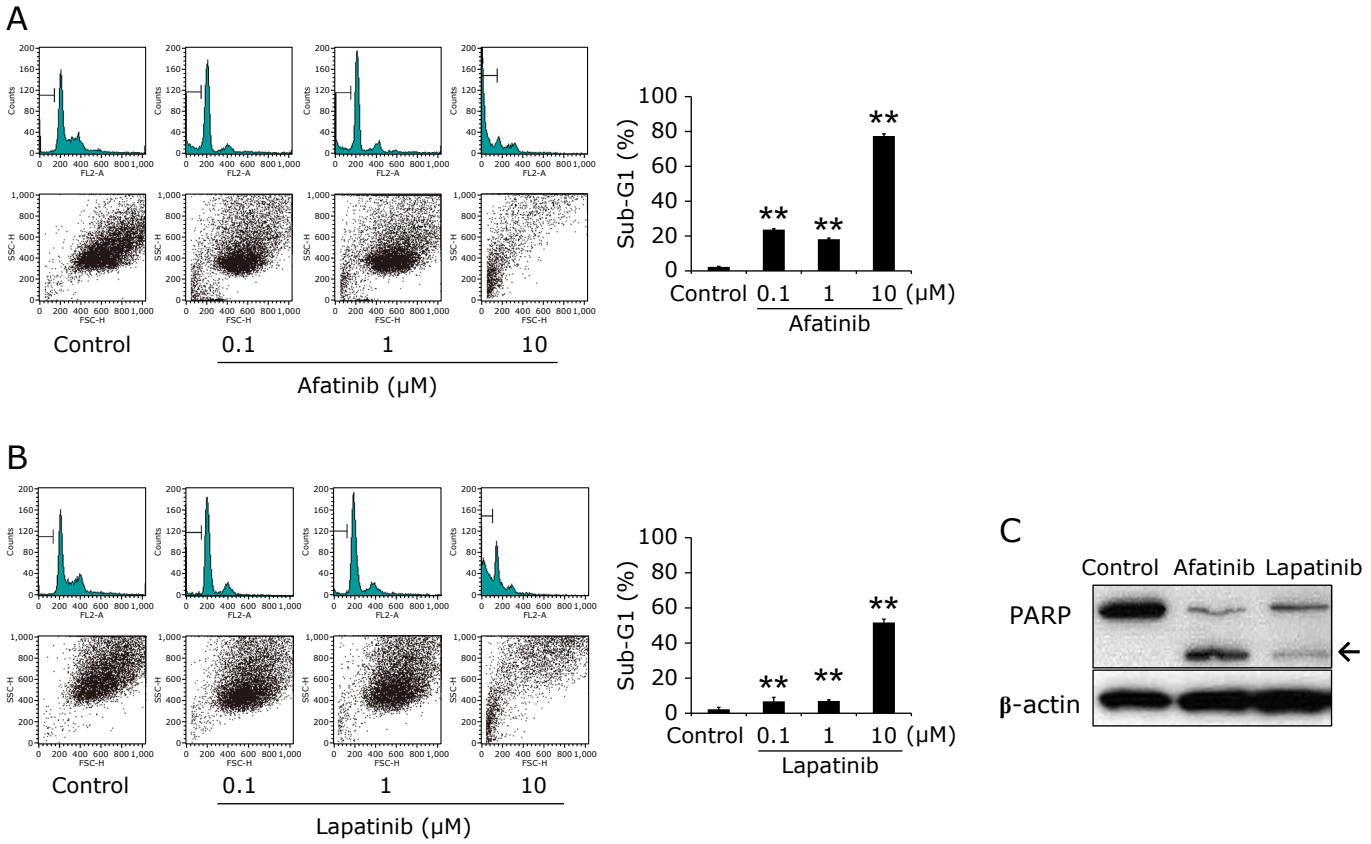

Fig. 2. EGFR inhibitors induce apoptosis in HaCaT cells. (A, B) Sub-G1 populations after treatment with afatinib or lapatinib. Cells were treated with 0.1, 1, or 10 μM afatinib (A) and 0.1, 1, or 10 μM lapatinib (B) for 72 h. The DNA content of cells was analyzed by flow cytometry. (C) Cleaved PARP after treatment with afatinib and lapatinib. Cells were treated with 10 μM afatinib or 10 μM lapatinib for 48 h, and cleaved PARP was analyzed by western blotting. β-Actin was used as a loading control. Columns, means of triplicate data; bars, SD; **p<0.01.

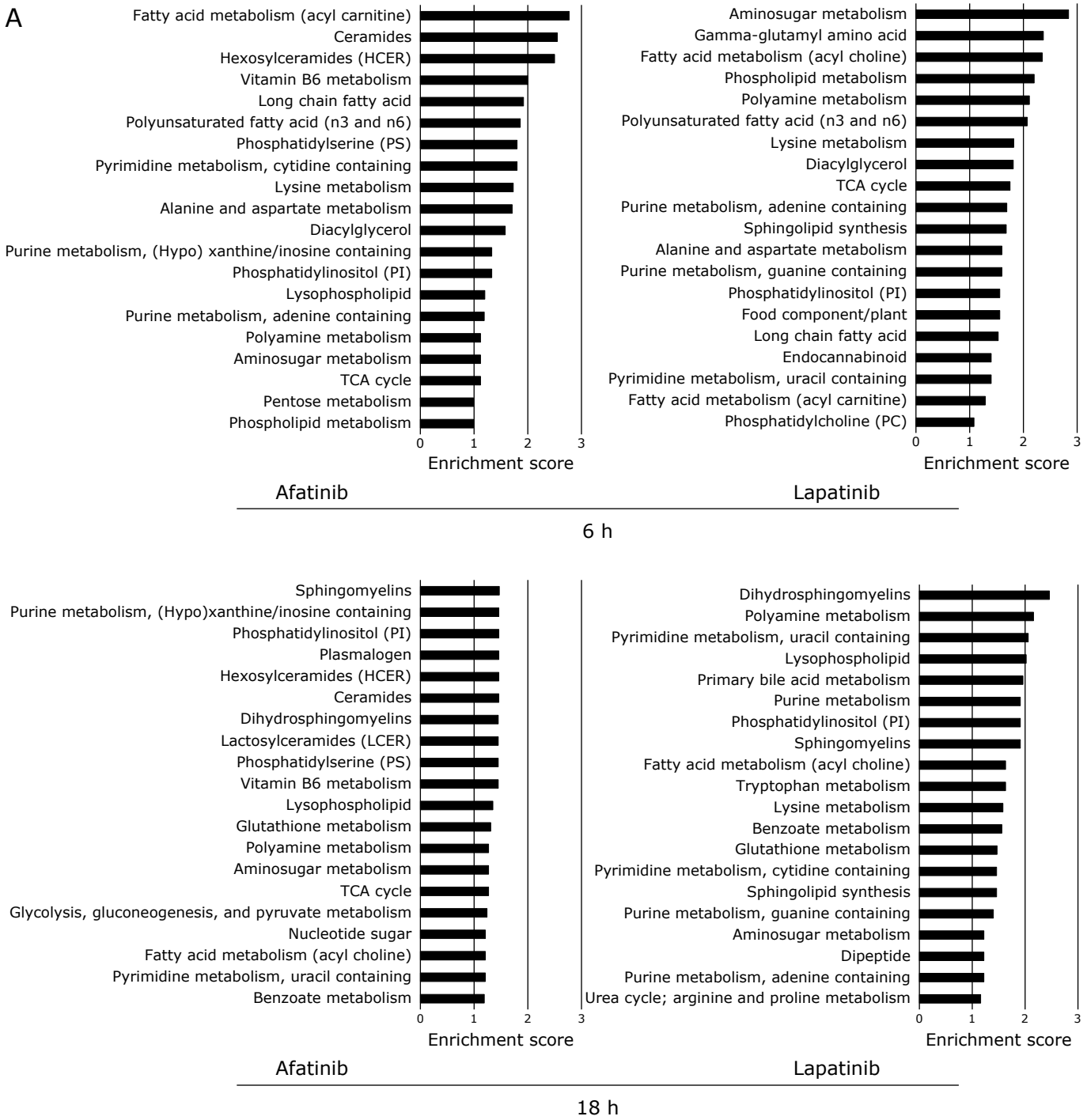

Fig. 3. EGFR inhibition induces metabolic changes in HaCaT cells and their supernatant. (A) Signal enrichment analysis of the metabolites detected in this study. The sub-pathway groups were ranked according to their enrichment scores. Top 20 sub-pathways are on the list. HaCaT cells were treated with 10 μM afatinib and lapatinib for the indicated times. (B) Heatmap of significant biochemicals profiled in this study. HaCaT cells were treated with 10 μM afatinib and lapatinib for the indicated times. The red- and green-shaded cells indicate $p<0.05$ (red and green indicate that the mean values are significantly higher and lower, respectively, compared to the control). The light red- and light green-shaded cells indicate $0.05<p<0.10$ (light red and light green indicate that the mean values trend higher and lower, respectively, compared to the control). Non-colored cells did not significantly differ in this comparison, and missing values are imputed with the minimum. (C) Schematic images of cell metabolic pathways for energy production: glycolysis, lipolysis, β-oxidation, TCA cycle, and ketogenesis. See color figure in the on-line version.

Treatment with afatinib (Fig. 2A) and lapatinib (Fig. 2B) resulted in almost dose-dependent increases in the sub-G1 populations. Furthermore, in western blotting analysis, we observed cleavage of PARP in the EGFR inhibitor-treated HaCaT cells (Fig. 2C). Accordingly, EGFR inhibitors induced apoptosis in HaCaT cells.

Metabolome analysis revealed escalation of oxidative stress in EGFR inhibitor-treated cells. To explore the detailed mechanisms of the cytotoxicity induced by EGFR inhibitors, we next performed metabolomics analysis. After treatment with

doi: 10.3164/jcbn.20-112

B

Super pathway	Sub pathway	Biochemical name	6 h		18 h	
			Afatinib	Lapatinib	Afatinib	Lapatinib
Energy	Glycolysis, Gluconeogenesis, and Pyruvate Metabolism	glucose	1.11	1.15	1.65	1.09
		dihydroxyacetone phosphate (DHAP)	1.33	0.89	0.26	0.59
		3-phosphoglycerate	1.43	0.64	0.19	0.32
		phosphoenol-pyruvate (PEP)	1.30	0.54	0.17	0.35
		pyruvate	1.51	1.65	2.16	1.09
		lactate	1.12	1.01	1.38	1.27
		glycerate	1.24	0.94	1.02	0.92
	Pentose Phosphate Pathway	sedoheptulose-7-phosphate	1.11	1.05	0.65	0.66
	TCA Cycle	citrate	1.13	0.85	2.80	1.89
		aconitate [cis or trans]	1.01	0.71	2.18	2.00
		alpha-ketoglutarate	1.13	0.84	1.99	0.72
		succinylcarnitine (C4-DC)	1.36	1.30	3.65	1.61
		succinate	1.06	2.62	0.61	0.85
		fumarate	1.26	1.34	0.80	0.97
		malate	1.30	1.40	0.78	0.99
		2-methylcitrate/ homocitrate	1.49	1.49	1.47	1.23
	Oxidative Phosphorylation	acetylphosphate	1.10	0.66	0.37	0.69
		phosphate	1.79	1.67	0.95	0.96

Super pathway	Sub pathway	Biochemical name	6 h		18 h	
			Afatinib	Lapatinib	Afatinib	Lapatinib
Energy	Fatty Acid Metabolism (Acyl Carnitine)	acetylcarnitine (C2)	1.32	0.66	1.37	1.55
		hexanoylcarnitine (C6)	1.44	0.81	1.54	1.31
		laurylcarnitine (C12)	1.43	1.08	3.00	2.92
		myristoylcarnitine (C14)	4.40	1.14	4.14	3.53
		palmitoylcarnitine (C16)	11.18	2.19	5.13	1.78
		palmitoleoylcarnitine (C16:1)	2.56	1.28	1.23	1.38
		stearoylcarnitine (C18)	8.99	2.40	9.93	1.69
		linoleoylcarnitine (C18:2)	2.91	1.62	1.15	1.24
		oleoylcarnitine (C18:1)	6.38	1.46	3.17	1.50
		myristoleoylcarnitine (C14:1)	1.75	1.69	0.70	1.55
		arachidoylcarnitine (C20)	5.52	3.21	5.67	1.94
		arachidonoylcarnitine (C20:4)	3.49	2.98	1.23	0.82
		behenoylcarnitine (C22)	4.51	3.07	3.93	1.59
		dihomo-linolenoylcarnitine (C20:3n3 or 6)	2.19	1.26	3.13	0.86
		dihomo-linoleoylcarnitine (C20:2)	3.70	1.00	10.06	1.74
		eicosenoylcarnitine (C20:1)	3.81	1.41	6.98	1.58
		erucoylcarnitine (C22:1)	2.73	1.33	6.20	1.73
		docosapentaenoylcarnitine (C22:5n3)	3.31	1.43	3.22	0.79
		lignoceroylcarnitine (C24)	3.19	3.37	2.06	1.77
		margaroylcarnitine (C17)	7.88	1.71	8.18	1.81
		nervonoylcarnitine (C24:1)	5.65	3.51	2.93	1.47
		cerotoylcarnitine (C26)	2.01	2.38	1.82	2.01
		ximenoylcarnitine (C26:1)	3.91	3.81	2.00	1.99
		pentadecanoylcarnitine (C15)	5.19	1.32	3.68	2.10
	Carnitine Metabolism	deoxycarnitine	1.35	1.45	0.70	1.12
		carnitine	1.69	1.49	2.73	1.35
	Ketone Bodies	3-hydroxybutyrate (BHBA)	1.41	1.03	1.96	1.38

C

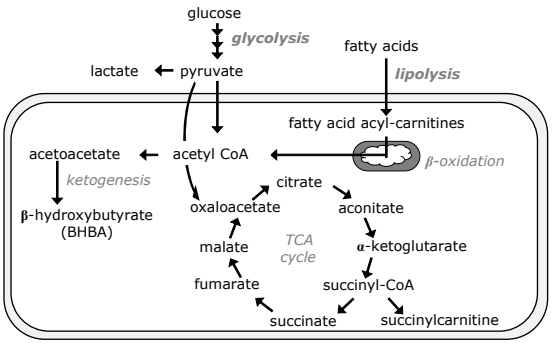

Fig. 3. continued

afatinib or lapatinib for 6 or 18 h, HaCaT cells and supernatants were separately collected and analyzed by Metabolon, Inc. Consequently, 676 metabolites and compounds in cells and 482 in the supernatants were detected (Supplemental Table 1*). In intracellular pathway enrichment analysis (Fig. 3A), TCA cycle and acylcarnitines are listed up on the high order of both afatinib and lapatinib ranking. These terms are related to energy production in cells (Fig. 3B and C). Although acetyl-CoA, a starting metabolome of the TCA cycle, was not determined in this study, pyruvate was increased (Fig. 3B left panel). Pyruvate is one of the end products of glycolysis and the main input of the TCA cycle. The other metabolites related to the TCA cycle were somewhat increased (Fig. 3B left panel), indicating that the TCA cycle was activated and mitochondrial respiratory chain was up-regulated in EGFR-inhibited HaCaT cells. Moreover, the levels of acylcarnitines and carnitines, which transport fatty acids into the mitochondria and mediate β-oxidation, were significantly higher in cells treated with EGFR inhibitors compared to in control cells (Fig. 3B, right panel). The end product of β-oxidation, 3-hydroxybutyrate, was significantly increased (Fig. 3B, bottom right panel). The behaviors of these metabolites suggested that β-oxidation was increased in EGFR inhibitor-treated skin cells. Acceleration of the TCA cycle and β-oxidation would have resulted in increased mitochondrial ROS production. In contrast, the pentose phosphate pathway, which plays an important role in scavenging ROS, was significantly reduced by EGFR inhibition at 18 h (Fig. 3B, left panel), suggesting that detoxification of ROS was impeded. Consequently, the accumulation of mitochondrial ROS was predicted in EGFR inhibitor-treated skin cells.

We then focused on changes in glutathione, which is known to exist in reduced (GSH) and oxidized (GSSG) states, and the ratio of GSSG to GSH is used to evaluate ROS accumulation. In metabolomics analysis, although EGFR inhibitors significantly decreased the intracellular levels of GSH in HaCaT cells (Fig. 4A), increased levels of GSSG were observed in the supernatant (Fig. 4B). The intracellular GSSG/GSH ratio tended to be increased after treatment with afatinib and lapatinib (Supplemental Fig. 1*). Accordingly, we additionally carried out intracellular GSSG/GSH quantification analysis after metabolomics analysis. Our results confirmed the almost dose-dependent increase in the GSSG/GSH ratio in EGFR inhibitor-treated HaCaT cells (Fig. 4C).

Accumulation of ROS was partly involved in afatinib-induced apoptosis. We next evaluated the contribution of ROS to EGFR inhibition-induced apoptosis in HaCaT cells. We first detected accumulation of ROS using H2DCFDA, an ROS indicator. The relative levels of ROS were significantly increased after treatment with afatinib (Fig. 5A) and lapatinib (Fig. 5B). To clarify the contribution of ROS to afatinib-induced apoptosis, we treated HaCaT cells with afatinib in the absence or presence of NAC, an ROS scavenger. Supplementation with NAC partly but significantly rescued cells from afatinib-induced apoptosis (Fig. 5C). Taken together, apoptosis of skin cells induced by EGFR inhibition was at least partly dependent on the increase in oxidative stress.

*See online. https://doi.org/10.3164/jcbn.20-112

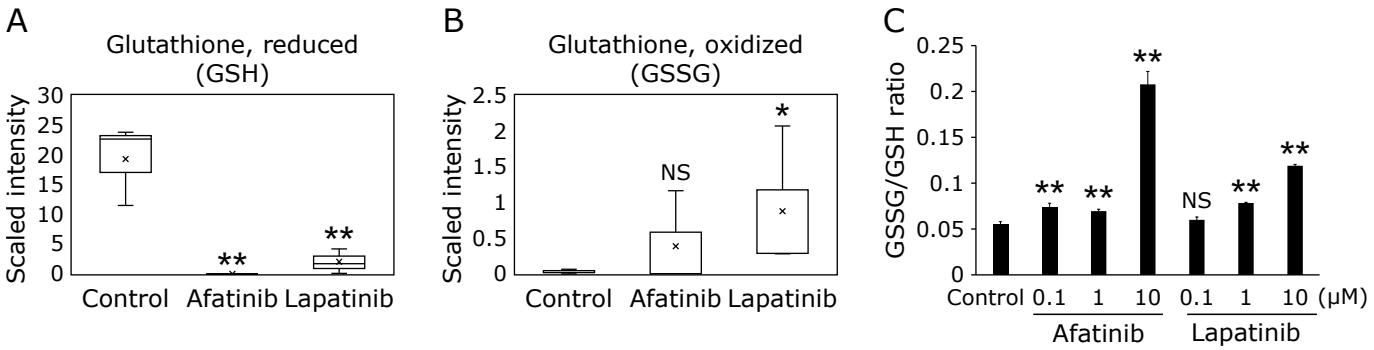

Fig. 4. Alterations in oxidative stress-related metabolites. (A, B) Metabolomics changes in glutathione. (A) Reduced glutathione (GSH) in EGFR inhibitor-treated HaCaT cells. Cells were treated with 10 μM afatinib or 10 μM lapatinib for 18 h. (B) Oxidized glutathione (GSSH) in the supernatant. Cells were treated with 10 μM afatinib or 10 μM lapatinib for 18 h. Boxes, limit of lower to upper quartiles; middle bar in a box, median value; badge mark, mean value; vertical lines, minimum to maximum of distributions; *p<0.10; **p<0.05. (C) Dose-dependent changes in the intracellular ratio of GSSG to GSH glutathione in EGFR inhibitor-treated HaCaT cells. The ratio was calculated based on data using a GSSG/GSH quantifying kit. Cells were treated with or without 0.1, 1, or 10 μM afatinib or 0.1, 1, or 10 μM lapatinib for 18 h. Columns, means of triplicate data; bars, SD; **p<0.01.

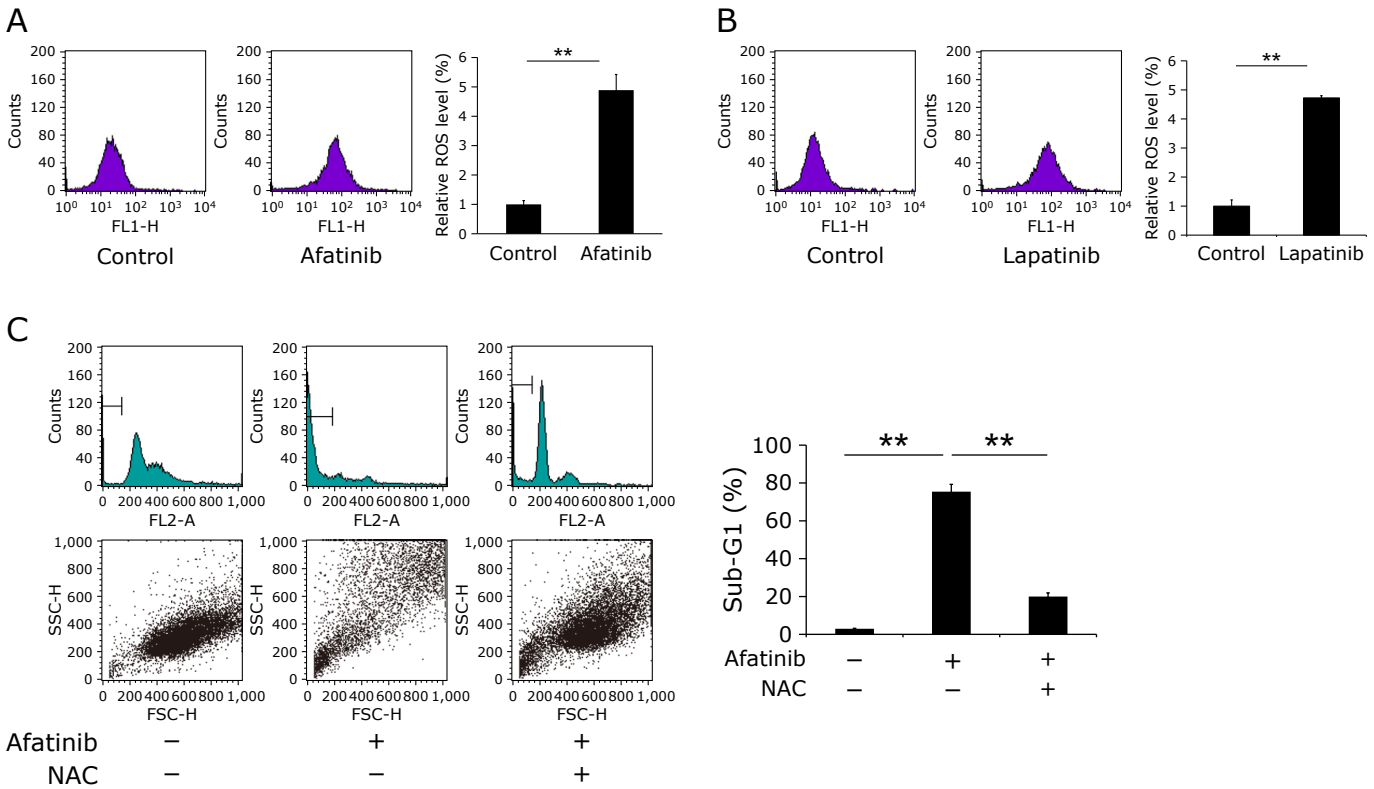

Fig. 5. ROS is partly involved in afatinib-associated apoptosis of HaCaT cells. (A, B) Intracellular levels of ROS in cells treated with or without EGFR inhibitors. HaCaT cells were treated with 10 μM afatinib (A) or lapatinib (B) for 6 h, and then stained with CM-H2DCFDA prior to flow cytometric analysis. (C) Sub-G1 population after treatment with afatinib with or without NAC. Cells were treated with 10 μM afatinib in the presence or absence of 5 mM NAC for 72 h. Columns, means of triplicate data; bars, SD; **p<0.01.

Discussion

We observed that EGFR inhibition triggered perturbed metabolism in keratinocyte cells, including an increase in the GSSG/GSH ratio, indicating the accumulation of ROS. Our study suggests that the mechanism of the cutaneous side effects associated with administration of EGFR inhibitors can be partly explained by induction of ROS-mediated apoptosis.

ROS levels are known to be balanced by their generation and detoxification. Our data suggest that the TCA cycle and β-oxidation were increased and the pentose phosphate pathway was suppressed. The TCA cycle is the main component of the mitochondrial respiratory chains, which produce ROS during energy production. β-Oxidation is also a major source of ROS production in cells.[19] The pentose phosphate pathway plays an important role in scavenging ROS not only in cancer [20] but also in skin cells.[21] Thus, EGFR inhibition may lead to both production of *de novo* ROS and suppression of ROS

doi: 10.3164/jcbn.20-112

scavenging, resulting in the accumulation of oxidative stress. Notably, ROS-dependent apoptosis was involved in skin cell damage by EGFR inhibitors, which was further demonstrated by add-back experiments in which NAC inhibited apoptosis induced by afatinib (Fig. 5C). As to the difference in the IC50 values between afatinib and lapatinib, ROS might have played an important role. Namely, considering that afatinib covalently binds to cysteine number 797 of the EGFR, there is a possibility that afatinib also directly bound to GSH and inhibited its ability of anti-oxidation. Indeed, afatinib almost eliminated GSH in HaCaT cells (Fig. 4A), and the GSSG/GSH ratio was higher in the afatinib treated HaCaT cells comparing to that of the lapatinib (Fig. 4C).

The present study obtained some other interesting findings on metabolomic alterations in skin cells treated with EGFR inhibitors. EGFR inhibitor-treated cells showed significantly higher levels of kynurenine and kynurenate following exposure to lapatinib or afatinib (Supplemental Fig. 2B*), suggesting activation of the tryptophan-kynurenine pathway. In keratinocyte cells, kynurenine is known to be generated from tryptophan through the action of indoleamine 2,3-dioxygenase.[22] Briefly, this enzyme is activated by stimulation with UV or inflammatory cytokines, such as interleukin-1, interleukin-6, interleukin-8, interferon-γ, and tumor necrosis factor α.[23] As HaCaT cells were not co-incubated with immune cells in our study, we considered that HaCaT cells themselves secreted inflammatory cytokines, inducing inflammatory-like reactions in cells. Indeed, keratinocyte cells are known to secrete these inflammatory molecules.[24–26] These autocrine or paracrine mechanisms may also be involved in severe skin inflammatory reactions under physiological conditions during treatment with EGFR inhibitors.

In conclusion, our results not only improve the understanding of EGFR inhibition-induced accumulation of ROS and skin cell toxicity, but also provide a therapeutic avenue for managing EGFR-inhibition associated cutaneous side effects. Detoxifying ROS may be an effective approach for treating cutaneous side effects; however, ROS play an important role in cancer treatment.[27] EGFR inhibitor-associated ROS production in cancer cells is related to delayed drug resistance, prevention of epithelial-mesenchymal transition, and apoptosis.[28] Thus, effective treatment approaches should not impede the systemic cancer treatment effects of EGFR inhibitors while treating skin damage. For example, an ointment containing some ROS-scavenging agents may be a good local therapeutic strategy. For instance, NAC is a feasible candidate, as it is already clinically used as a safe and an inexpensive drug.[29,30] Improving the understanding of perturbations in metabolomics caused by EGFR inhibition may lead to strategies for preventing or curing EGFR inhibitor-associated cutaneous side effects.

Author Contributions

Study concept and design; MI-O and TT
Acquisition of data; MM, MI-O, CK, DK, FK, and YO
Drafting of the manuscript; MM, MI-O, TN, and MW
Critical revision of the manuscript; KS, TN, MW, and TT

Acknowledgments

This work was supported by a Grant-in-Aid for Scientific Research (C) 26461956 and Boehringer Ingelheim Japan.

We would like to thank Editage (www.editage.com) for their assistance with English language editing.

Abbreviations

EGFR	epidermal growth factor receptor
GSH	reduced glutathione
GSSG	oxidized glutathione
NAC	*N*-acetylcysteine
PARP	poly (ADP-ribose) polymerase
ROS	reactive oxygen species

Conflict of Interest

TT received research funding from Chugai, Daiichi Sankyo, and Eisai, and a lecture fee from Chugai, Daiichi Sankyo, Eisai, and Kyowa Kirin.

The other authors declare no conflicts of interest associated with this manuscript.

References

1 Seshacharyulu P, Ponnusamy MP, Haridas D, Jain M, Ganti AK, Batra SK. Targeting the EGFR signaling pathway in cancer therapy. *Expert Opin Ther Targets* 2012; **16**: 15–31.
2 Wee P, Wang Z. Epidermal growth factor receptor cell proliferation signaling pathways. *Cancers (Basel)* 2017; **9**: 52.
3 Huang SM, Harari PM. Epidermal growth factor receptor inhibition in cancer therapy: biology, rationale and preliminary clinical results. *Invest New Drugs* 1999; **17**: 259–269.
4 Normanno N, Maiello MR, De Luca A. Epidermal growth factor receptor tyrosine kinase inhibitors (EGFR-TKIs): simple drugs with a complex mechanism of action? *J Cell Physiol* 2003; **194**: 13–19.
5 Nicholson RI, Gee JM, Harper ME. EGFR and cancer prognosis. *Eur J Cancer* 2001; **37** Suppl 4: S9–S15.
6 Sihto H, Puputti M, Pulli L, *et al*. Epidermal growth factor receptor domain II, IV, and kinase domain mutations in human solid tumors. *J Mol Med (Berl)* 2005; **83**: 976–983.
7 Salomon DS, Brandt R, Ciardiello F, Normanno N. Epidermal growth factor-related peptides and their receptors in human malignancies. *Crit Rev Oncol Hematol* 1995; **19**: 183–232.
8 Holcmann M, Sibilia M. Mechanisms underlying skin disorders induced by EGFR inhibitors. *Mol Cell Oncol* 2015; **2**: e1004969.
9 Lacouture ME. Mechanisms of cutaneous toxicities to EGFR inhibitors. *Nat Rev Cancer* 2006; **6**: 803–812.
10 Robert C, Soria JC, Spatz A, *et al*. Cutaneous side-effects of kinase inhibitors and blocking antibodies. *Lancet Oncol* 2005; **6**: 491–500.
11 Chanprapaph K, Vachiramon V, Rattanakaemakorn P. Epidermal growth factor receptor inhibitors: a review of cutaneous adverse events and management. *Dermatol Res Pract* 2014; **2014**: 734249.
12 Pastore S, Lulli D, Girolomoni G. Epidermal growth factor receptor signalling in keratinocyte biology: implications for skin toxicity of tyrosine kinase inhibitors. *Arch Toxicol* 2014; **88**: 1189–1203.
13 Mascia F, Lam G, Keith C, *et al*. Genetic ablation of epidermal EGFR reveals the dynamic origin of adverse effects of anti-EGFR therapy. *Sci Transl Med* 2013; **5**: 199ra110.
14 Lichtenberger BM, Gerber PA, Holcmann M, *et al*. Epidermal EGFR controls cutaneous host defense and prevents inflammation. *Sci Transl Med* 2013; **5**: 199ra111.
15 Uchi H, Terao H, Koga T, Furue M. Cytokines and chemokines in the epidermis. *J Dermatol Sci* 2000; **24** Suppl 1: S29–S38.
16 Mascia F, Mariani V, Girolomoni G, Pastore S. Blockade of the EGF receptor induces a deranged chemokine expression in keratinocytes leading to enhanced skin inflammation. *Am J Pathol* 2003; **163**: 303–312.
17 Iizuka-Ohashi M, Watanabe M, Sukeno M, *et al*. Blockage of the mevalonate pathway overcomes the apoptotic resistance to MEK inhibitors with suppressing the activation of Akt in cancer cells. *Oncotarget* 2018; **9**: 19597–19612.
18 Miyamoto K, Watanabe M, Boku S, *et al*. xCT Inhibition increases sensitivity to vorinostat in a ROS-dependent manner. *Cancers (Basel)* 2020; **12**: 827.
19 Poirier Y, Antonenkov VD, Glumoff T, Hiltunen JK. Peroxisomal beta-oxidation—a metabolic pathway with multiple functions. *Biochim Biophys*

*See online. https://doi.org/10.3164/jcbn.20-112

Acta 2006; **1763**: 1413–1426.
20 Patra KC, Hay N. The pentose phosphate pathway and cancer. *Trends Biochem Sci* 2014; **39**: 347–354.
21 Kuehne A, Emmert H, Soehle J, *et al*. Acute activation of oxidative pentose phosphate pathway as first-line response to oxidative stress in human skin cells. *Mol Cell* 2015; **59**: 359–371.
22 Sheipouri D, Grant R, Bustamante S, Lovejoy D, Guillemin GJ, Braidy N. Characterisation of the kynurenine pathway in skin-derived fibroblasts and keratinocytes. *J Cell Biochem* 2015; **116**: 903–922.
23 Sheipouri D, Braidy N, Guillemin GJ. Kynurenine pathway in skin cells: implications for UV-induced skin damage. *Int J Tryptophan Res* 2012; **5**: 15–25.
24 Gröne A. Keratinocytes and cytokines. *Vet Immunol Immunopathol* 2002; **88**: 1–12.
25 Bashir MM, Sharma MR, Werth VP. TNF-alpha production in the skin. *Arch Dermatol Res* 2009; **301**: 87–91.
26 Howie SE, Aldridge RD, McVittie E, Forsey RJ, Sands C, Hunter JA. Epidermal keratinocyte production of interferon-gamma immunoreactive protein and mRNA is an early event in allergic contact dermatitis. *J Invest Dermatol* 1996; **106**: 1218–1223.
27 Postovit L, Widmann C, Huang P, Gibson SB. Harnessing oxidative stress as an innovative target for cancer therapy. *Oxid Med Cell Longev* 2018; **2018**: 6135739.
28 Teppo HR, Soini Y, Karihtala P. Reactive oxygen species-mediated mechanisms of action of targeted cancer therapy. *Oxid Med Cell Longev* 2017; **2017**: 1485283.
29 World Health Organization Model List of Essential Medicines. The Expert Committee on the Selection and Use of Essencial Medicines. https://www.who.int/medicines/publications/essentialmedicines/en/. Accessed 1 July 2020.
30 Hitchings A, Lonsdale D, Burrage D, Baker E. *Top 100 Drugs: Clinical Pharmacology and Practical Prescribing (2nd ed.)*. Elsevier, 2018; 22–23.

doi: 10.3164/jcbn.20-112